Journal of Materials Chemistry A

Accepted Manuscript

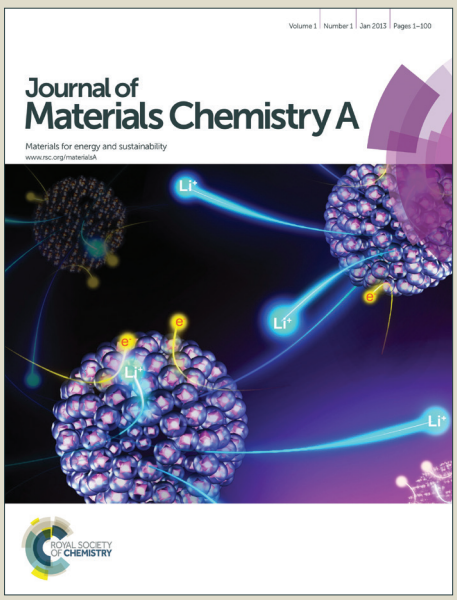

ROYAL SOCIETY OF CHEMISTRY

www.rsc.org/materialsA

Organic Solvent Vapor Sensitive Methylammonium Lead Trihalide Film Formation for Efficient Hybrid Perovskite Solar Cells

Jiarong Lian[1,2] Qi Wang[1], Yongbo Yuan[1], Yuchuan Shao[1] and Jinsong Huang[1]*

[1] Department of Mechanical and Materials Engineering and Nebraska Center for Materials and Nanoscience, University of Nebraska-Lincoln, Lincoln, Nebraska 68588-0656.

[2] Key Laboratory of Optoelectronic Devices and Systems of Ministry of Education and Guangdong Province, College of Optoelectronic Engineering, Shenzhen University, Shenzhen China, 518060.

Abstract: The anisotropic electronic properties of the perovskite crystals originating from to their non-cubic crystal structures can potentially give rise to the grain orientation correlated photovoltaic device performance. Here we report that organic solvent vapor atmosphere introduced during the spin-coating and formation of perovskite film changes the orientation and size of perovskite grains. It was found that slightly larger but much more oriented methylammonium lead trihalide grains ($CH_3NH_3PbI_3$) grains could be obtained under 1, 2-Dichlorobenzene (DCB) and Dimethyl sulfoxide (DMSO) vapor atmosphere. The devices with more oriented grains outperformed regular devices with more random grains by 50 mV larger open circuit voltage as well as slightly increased fill factor. The device efficiency enhancement can be attributed to the longer charge recombination lifetime resulting from the reduced trap density and oriented grains. This result is important in providing the guideline in comparing the results from various groups because organic solvent vapors generally present in the sealed glovebox for perovskite solar cell fabrication.

[1] * To whom correspondence should be addressed-mail: jhuang2@unl.edu

A class of compounds named organometal trihalide perovskites (OTPs) that were first uncovered in the Ural Mountains more than a century ago, right now is a rock star in the field of solar-energy research, which exhibits numerous appealing features, including very strong light absorption, large bipolar carrier mobility, free charge generation under illumination, and long exciton diffusion lengths [1-3]. The OTP devices have showed unprecedented climbing in power conversion efficiency (PCE) from the first 3.8% in 2009 [4], to that of around 10% in 2012 [5], and a certified efficiency of 20.1% in early 2015 [6]. By analyzing the attainable photocurrent and photovoltage, increasing perovskite solar cells to 30% is also realistic with a tandem structure with well-established c-Si solar cells [7]. Therefore, their high efficiencies and low-cost solution process make perovskite solar cells an extremely commercially attractive option [8].

The quality of perovskite films, such as morphology and crystallinity, has been shown to strongly influence the overall photovoltaic performance of devices [1, 9]. The preferred hybrid perovskite films to date fulfill several criteria: high film uniformity, complete film coverage without pin-holes, and large perovskite crystallite grains, to harness their excellent carrier transport properties [9, 10]. Many efforts have been devoted to improve film morphology and coverage via optimizing fabrication protocols during the film formation process, including precursor composition changing [5, 11], solvent engineering [12, 13], deposition & annealing temperature optimizing etc [14, 15]. We reported a simple method to form the most continuous, compact iodine perovskite ($CH_3NH_3PbI_3$, $MAPbI_3$) films by the interdiffusion of spin-coated stacking layers of PbI_2 and MAI assisted by thermal annealing [16]. To increase perovskite crystallinity and grain size, some additives are incorporated to facilitate homogenous nucleation and modulate the kinetics of growth during crystallization [1], and a solvent annealing method has also been developed by us [10].

In our previous study of using solvent-annealing to enhance polycrystalline film grain size, the organic solvent vapors were introduced during thermal annealing process of perovskite layers. Since the solid perovskite films already formed after 90 second thermal annealing, the solvent vapors in the solvent annealing is expected to facilitate the grain growth and grain coalescence by providing a higher ion diffusion mobility environment. In this study, we introduce the solvent vapor during the perovskite formation stage which is the spin-coating of MAI on PbI_2. According to the formation process of perovskite film by the two-step interdiffusion method, the perovskite nucleation is expected to occur first at MAI/PbI_2 interface [16]. It was found that both larger and oriented grains could be obtained for $MAPbI_3$ film by introducing 1,2-Dichlorobenzene (DCB) and Dimethyl sulfoxide (DMSO) atmosphere. DMSO and DCB were chosen because they are frequently used solvents in device fabrication and vapor of these solvents always presents in gloveboxes. Therefore understanding the influence of these solvent vapors on film morphology and device performance provides insight in comparing the device performance in many labs.

The solvent vapor modulated spin-coating process of the PbI_2/MAI stacking layer is illustrated in **Figure 1**. For the film fabrication, PbI_2 and MAI were first dissolved dimethylformamide (DMF) and isopropanol (IPA) with a concentration of 400 mg/ml and 40 mg/ml, respectively. Poly(3,4-ethylenedioxythiophene)poly(styrenesulfonate) (PEDOT:PSS) was spin coated on the pre-cleaned indium tin oxide (ITO) glass substrate at a spin-rate of 3,000 rpm for 60 seconds. The 25 nm thick PEDOT:PSS films were annealed at 135 °C for 20 minutes. Hot PbI_2 precursor solution (70 °C) was spin-coated on the PEDOT:PSS surface at a spin-rate of 6,000 rpm for 35 seconds in nitrogen filled glove-box, then the PbI_2 films were dried at 70 °C for 15 minutes. Here the DCB and DMSO solvent vapors were generated by heating the solvent-

filled flask (150 µl DCB or DMSO in 50 ml size flask) at 100 °C, and the evaporated solvent vapor was guided via a tube onto the top of the PbI_2 films. It is noted that DMSO additive [12] was used to engineering the kinetics of grain growth. The difference here is DMSO or DCB were introduced in vapor phase, which explains the influence of vapor environment in device fabrication. After the PbI_2 films were soaked by the vapor for about 15 seconds, the MAI solution was spin-coated on the top of PbI_2 films at a spin-rate of 6,000 rpm for 35 seconds. The spin-coated MAI layers were dried at 70 °C for 10 minutes, and further annealed at 100 °C for 60 minutes. In order to passivate the surface defects of the perovskite films, 20 nm thickness phenyl-C61-butyric acid methyl ester (PCBM) films were coated on the perovskite layers. After that, 20 nm C_{60}, 7 nm 2,9-dimethyl-4,7-diphenyl-1,10-phenanthroline (BCP) and 100 nm aluminum layers were sequentially deposited by thermal evaporation. The resulted devices have a structure of ITO/PEDOT: PSS (25 nm)/$MAPbI_3$ (280 nm)/PCBM (20 nm)/C_{60} (20 nm)/BCP (8 nm)/Al (100 nm).

The influence of the organic solvent vapor treatment during film formation process on the morphology and microstructure of the $MAPbI_3$ films were examined by scanning electron microscopy (SEM) and X-ray diffraction (XRD). As shown in **Figure 2**, DCB and DMSO vapor treated $MAPbI_3$ films show slightly larger grains than those of the control $MAPbI_3$ film formed under N_2 atmosphere with average grain size increased from 180 nm to 230 nm and 300 nm, respectively. The XRD measurement results shown in **Figure 3** also show stronger diffraction peak intensity for the DCB and DMSO vapor treated $MAPbI_3$ films, which indicates the better crystallinity of the solvent vapor treated $MAPbI_3$ films. The mean coherently scattering domains size calculated from the half width of the XRD peaks according to Debye-Scherrer formula

increased from 60 nm for the N_2 treat $MAPbI_3$ film to 68 nm for the DCB vapor treated $MAPbI_3$ film, and to 76 nm for the DMSO vapor treated $MAPbI_3$ film, respectively.

By taking a closer look at the XRD spectra, one may find the relative intensity for each peak has changed, which indicates the grain orientation changes for these $MAPbI_3$ films. To illustrate the degree of grain orientation variation of the $MAPbI_3$ polycrystalline grains, we normalized the XRD peaks to the peak at 14.17°, i.e. the (110) plane, and plotted the spectra against the azimuth angle ω in **Figure 3b**. It is obvious that all the other XRD peaks for the planes except (110) plane, including (112), (202), (312), (224), and (314), have much lower intensity, which suggests increased (110) orientation of the polycrystalline $MAPbI_3$ films, and the long axis preferentially stayed parallel to the substrate for DCB and DMSO treated $MAPbI_3$ films. Here it should be noted that the regular thermal annealing and solvent-annealing treatments do not cause grain orientation change despite of the increasing grain size [10, 17, 18], which is absolutely different with our case using solvent spin coating method.

Because of the large size of the iodine atoms, the $MAPbI_3$ crystal should be tetragonal or orthorhombic with a distorted PbI_6^{4-} octahedral structure [19]. It is thus natural to hypothesize that $MAPbI_3$ crystals have anisotropic electronic properties. It is interesting to note that nearly all the high performance perovskite solar cells have the long axis of the $MAPbI_3$ films preferentially oriented parallel to the substrate, where the plane of (110), (220), and (330) exhibit the strongest intensity in the X-ray diffraction (XRD) spectra [5, 9, 10]. In addition, some other studies found that increasing immersion solution temperatures can realize the preferential orientation of (110) plane without changing the crystal size, and the corresponding devices achieve higher short circuit currents [20]. Saliba *et al.* also fabricated high performance devices with larger crystal size and more oriented domains via a flash annealing procedure, in which the samples were first

held at 100 °C for 5 min, then rapidly heated to 130 °C in <3 min, and held there for another 5 min [14]. These studies suggest that controlling the deposition parameters to achieve highly oriented crystalline domains can be a new route to enhance the efficiency of perovskite solar cells.

Photovoltaic devices were fabricated to evaluate the influence of enlarged grain size and increased (110) orientation on the device performance. **Figure 4** shows the photocurrent density (J) at different bias for the devices, and the performance of the devices was summarized in **Table 1.** DCB and DMSO treatments barely changed the short current density *(Jsc)*, but obviously increased open-circuit voltage (*Voc*) from 0.85 V to 0.90 V, and also enlarged the fill factor (*FF*) from 65.8% to more than 70%. The PCE is increased from 11.4% to 12.1% and 13.6% for the DCB and DMSO treated devices, respectively. It is noted these devices donot have the highest efficiency because of the different fabrication method used, for example, the solvent annealing was not applied in this study. All the three devices had the same series resistance (R_s) value of 70 Ohm/cm^2, but exhibit obviously different shunt resistance (R_{sh}). R_{sh} is an indication of the amount of current leakage paths in a solar cell device, which is caused by the crystal defects or impurities. Therefore the DMSO treated perovskite films, which show the largest R_{sh} of all three devices, should have the lowest concentration in crystal defects or impurities. This is consistent with the SEM and XRD measurement results. The largest grains in DMSO treated perovskite films give the lowest grain boundary area, and more oriented grains result in less large angle grain boundaries which can be highly leakage paths. The incident-photon-to-current conversion efficiency (IPCE) spectra of all the devices are similar, which is in good agreement with their comparable *Jsc*. Since the photocurrent hysteresis could cause inaccurate characterization of device efficiency, we further measured J-V curves with different scanning rates in the range of

0.02 V/s ~ 0.5 V/s and changed scanning directions with a scanning rate of 0.1 V/s. All the devices showed nearly the same J-V curves without obvious photocurrent hysteresis observed. This can be explained by the sophisticated passivation techniques we applied using the double layer fullerene [21].

The increase of device V_{oc} and *FF* can be explained by the reduction of traps density of DMSO and DCB treated perovskite films. The V_{oc} for the given photoactive materials is determined by the equation [22]:

$$V_{oc} = \frac{k_B T}{q} \ln(\frac{J_{sc}}{J_o}) \quad (1)$$

where k_B, T, q, J_{sc}, J_o stand for Boltzmann constant, absolute temperature, electron charge, short current density, and saturated reversed current density, respectively. The larger R_{sh} is expected to give a lower saturated reversed current density and thus enhance the device V_{oc}. The reduction of J_o can be correlated with the less defects and longer carrier lifetime since J_o is govern by

$$J_o = \frac{qWN_c^{1/2}N_v^{1/2}}{\sqrt{\tau_p \tau_n}} \exp[-\frac{E_g}{K_B T}] \quad (2)$$

where W, $N_{c(v)}$, *and* $\tau_{p(n)}$ are the total depletion width, effective conduction (valence) band density of states, and lifetime of minority holes (electrons), respectively.

To verify the less charge trap density and longer carrier lifetime in the DMSO and DCB treated perovskite films, we used thermal admittance spectroscopy (TAS) and impedance spectroscopy to directly measure trap density of states (*t*DOS) and charge recombination lifetime in device working conduction, i.e, under 1 sun illumination. TAS is an established and effective technique to measure the trap density in thin-film solar cells [23]. The experiment details and

calculations of the *t*DOS can be found elsewhere [10]. As shown in **Figure 5a**, the *t*DOS of the devices with DMSO treated perovskite films are obviously smaller than those treated in N_2 or DCB vapor. The total trap density, calculated by integrating the *t*DOS in the trap depth of 0.33 eV~0.41 eV, for DMSO treat device is 7.0×10^{15} m^{-3}, which is three-times smaller than that of the N_2 treat device (2.1×10^{16} m^{-3}). Therefore it is natural to correlate the reduced trap density with the enhanced device V_{oc} and *FF* because a lower trap density gives rise to a reduced charge recombination, which boosts V_{oc} and *FF*. Again the reduce trap density can be explained by the larger and oriented grains in DMSO treated perovskite films because grain boundaries are rich in defects based on our previous experimental and theoretical study [21]. The carrier recombination lifetime result, as shown in **Figure 5b**, is consistent with the trap density measurement result. The lower trap density in DMSO treated perovskite film gives a longer carrier recombination lifetime.

In summary, we have investigated the influence of solvent vapor introduced during spin-coating process on film morphology and associated device performance. It was found that slightly larger grain size but obviously preferred orientation of (110) plane for $MAPbI_3$ films were obtained for DCB and DMSO treated films., which contributed to the observed reduced trap density and longer carrier lifetime in these films. The photovoltaic performance of the devices with DCB and DMSO treated films also showed increased V_{oc} and *FF*, which can be explained by the lower trap density in these films. This study reveals the sensitivity of the perovskite film to the atmosphere during the formation of perovskite films, which is particularly important for comparing and interpreting the results from different research groups.

Acknowledgements

We thank the financial support from Department of Energy under Award DE-EE0006709 and the Nebraska Public Power District through the Nebraska Center for Energy Sciences Research,

Reference

[1] Liang P-W, Liao C-Y, Chueh C-C, Zuo F, Williams ST, Xin X-K, et al. Additive Enhanced Crystallization of Solution-Processed Perovskite for Highly Efficient Planar-Heterojunction Solar Cells. Advanced Materials. 2014;26:3748-54.

[2] Service RF. Perovskite Solar Cells Keep On Surging. Science. 2014;344:458.

[3] McGehee MD. Perovskite solar cells: Continuing to soar. Nat Mater. 2014;13:845-6.

[4] Kojima A, Teshima K, Shirai Y, Miyasaka T. Organometal halide perovskites as visible-light sensitizers for photovoltaic cells. Journal of the American Chemical Society. 2009;131:6050-1.

[5] Lee MM, Teuscher J, Miyasaka T, Murakami TN, Snaith HJ. Efficient Hybrid Solar Cells Based on Meso-Superstructured Organometal Halide Perovskites. Science. 2012;338:643-7.

[6] http://www.nrel.gov/ncpv/images/efficiency_chart.jpg. the National Renewable Energy Laboratory.

[7] Gao P, Gratzel M, Nazeeruddin MK. Organohalide lead perovskites for photovoltaic applications. Energy & Environmental Science. 2014;7:2448-63.

[8] http://www.wsj.com/articles/perovskite-offers-shot-at-cheaper-solar-energy-1411937799. Perovskite Offers Shot at Cheaper Solar Energy. The Wall Street Journal.

[9] Liu M, Johnston MB, Snaith HJ. Efficient planar heterojunction perovskite solar cells by vapour deposition. Nature. 2013;501:395-8.

[10] Xiao Z, Dong Q, Bi C, Shao Y, Yuan Y, Huang J. Solvent Annealing of Perovskite-Induced Crystal Growth for Photovoltaic-Device Efficiency Enhancement. Advanced Materials. 2014;26:6503-9.

[11] Abrusci A, Stranks SD, Docampo P, Yip H-L, Jen AKY, Snaith HJ. High-Performance Perovskite-Polymer Hybrid Solar Cells via Electronic Coupling with Fullerene Monolayers. NANO LETTERS. 2013;13:3124-8.

[12] Kim H-B, Choi H, Jeong J, Kim S, Walker B, Song S, et al. Mixed solvents for the optimization of morphology in solution-processed, inverted-type perovskite/fullerene hybrid solar cells. Nanoscale. 2014;6:6679-83.

[13] Chueh C-C, Liao C-Y, Zuo F, Williams ST, Liang P-W, Jen AKY. The roles of alkyl halide additives in enhancing perovskite solar cell performance. Journal of Materials Chemistry A. 2015.

[14] Saliba M, Tan KW, Sai H, Moore DT, Scott T, Zhang W, et al. Influence of Thermal Processing Protocol upon the Crystallization and Photovoltaic Performance of Organic–Inorganic Lead Trihalide Perovskites. The Journal of Physical Chemistry C. 2014;118:17171-7.

[15] Dualeh A, Tétreault N, Moehl T, Gao P, Nazeeruddin MK, Grätzel M. Effect of Annealing Temperature on Film Morphology of Organic–Inorganic Hybrid Pervoskite Solid-State Solar Cells. Advanced Functional Materials. 2014;24:3250-8.

[16] Xiao Z, Bi C, Shao Y, Dong Q, Wang Q, Yuan Y, et al. Efficient, high yield perovskite photovoltaic devices grown by interdiffusion of solution-processed precursor stacking layers. Energy & Environmental Science. 2014;7:2619-23.

[17] Bi C, Shao Y, Yuan Y, Xiao Z, Wang C, Gao Y, et al. Understanding the formation and evolution of interdiffusion grown organolead halide perovskite thin films by thermal annealing. Journal of Materials Chemistry A. 2014;2:18508-14.

[18] Tan KW, Moore DT, Saliba M, Sai H, Estroff LA, Hanrath T, et al. Thermally Induced Structural Evolution and Performance of Mesoporous Block Copolymer-Directed Alumina Perovskite Solar Cells. ACS Nano. 2014;8:4730-9.

[19] McLeod JA, Wu Z, Shen P, Sun B, Liu L. Self-Alignment of the Methylammonium Cations in Thin-Film Organometal Perovskites. The Journal of Physical Chemistry Letters. 2014;5:2863-7.

[20] Docampo P, Hanusch FC, Giesbrecht N, Angloher P, Ivanova A, Bein T. Influence of the orientation of methylammonium lead iodide perovskite crystals on solar cell performance. APL Materials. 2014;2:-.

[21] Shao Y, Xiao Z, Bi C, Yuan Y, Huang J. Origin and elimination of photocurrent hysteresis by fullerene passivation in CH3NH3PbI3 planar heterojunction solar cells. Nat Commun. 2014;5.

[22] Singh SC. Solar Photovoltaics : Fundamentals, Technologies and Applications: PHI Learning Pvt. Ltd.; 2011.

[23] Heath J, Zabierowski P. Capacitance Spectroscopy of Thin-Film Solar Cells. Advanced Characterization Techniques for Thin Film Solar Cells: Wiley-VCH Verlag GmbH & Co. KGaA; 2011. p. 81-105.

Table 1 the performance metrics extracted from J–V measurements under standard AM1.5G illumination (100 mW/cm^2) for the best device performance and average performance using different spin coating atmosphere.

Vapor Atmosphere		J_{sc} mA/cm^2	V_{oc} V	*PCE* %	*FF* %	R_s Ohm/cm^2	R_{sh} Ohm/cm^2
N_2	Best	19.25	0.86	11.35	68.5	70	1,425
	Average	19.32	0.85	10.80	65.7		
DCB	Best	19.04	0.90	12.13	70.6	70	3,071
	Average	19.02	0.90	12.09	70.6		
DMSO	Best	20.00	0.90	13.60	75.1	70	4,986
	Average	19.90	0.89	12.84	72.5		

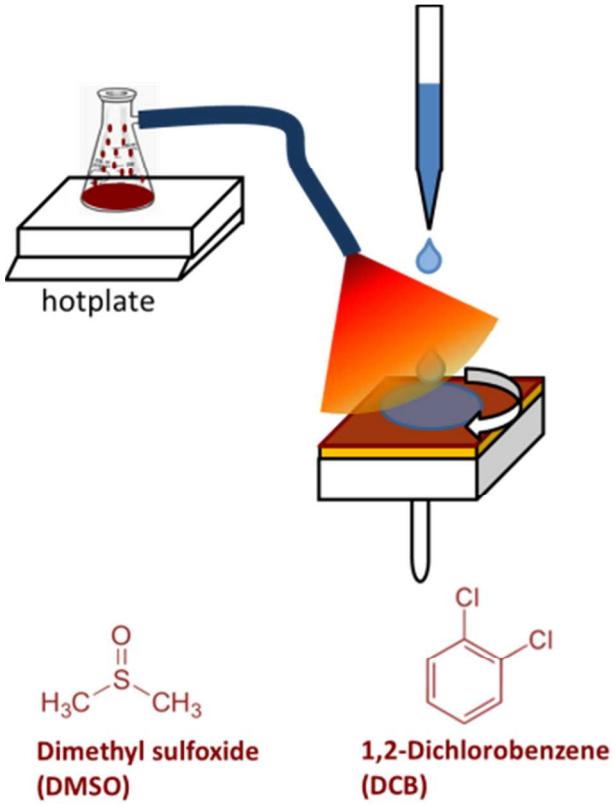

Figure 1 *Schematic illustration of the solvent spin-coating process where the solvent vapor was generated by heating DMSO and DCB solvents and directing the vapor by a tube to the film surface during spin-coating process. The chemical structures of DMSO and DCB solvents* were also shown.

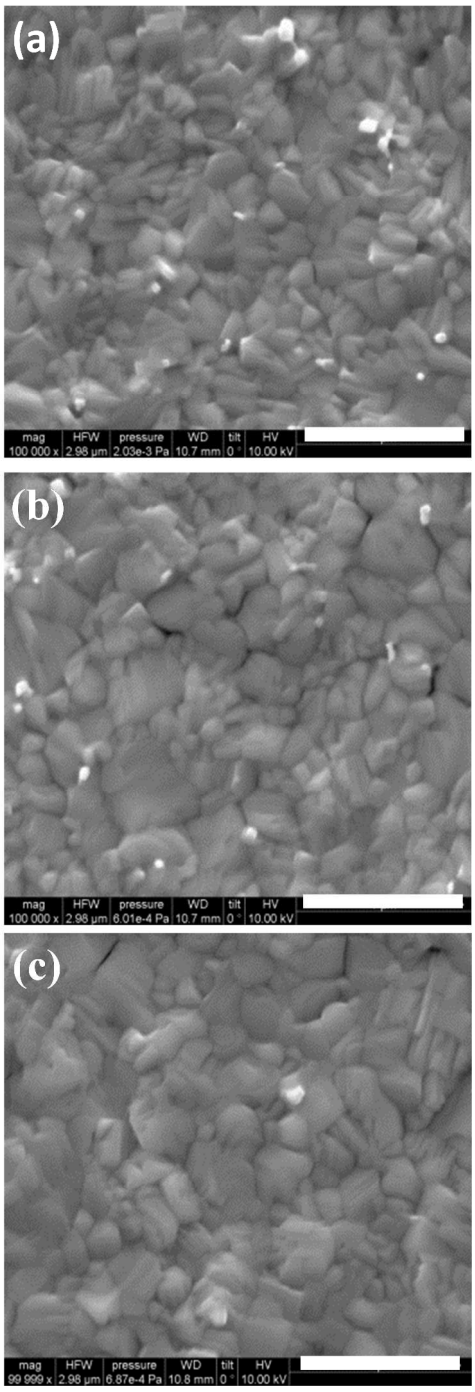

Figure 2 *The surface topography measured by SEM for different perovskite films fabricated in the atmosphere of (a) N_2, (b) DCB vapor, and (c) DMSO vapor, respectively. The scale bar is 1 µm.*

(a)

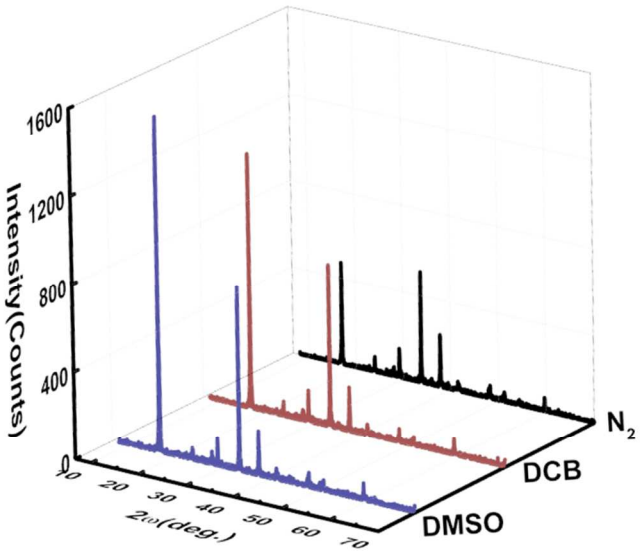

(b)

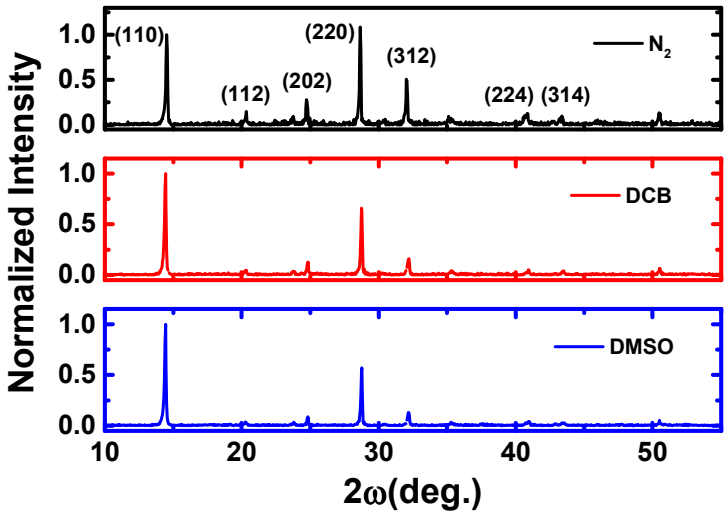

Figure 3 *(a) The absolute and (b) normalized intensity X-ray diffraction spectra of perovskite samples fabricated in N_2, DCB, and DMSO condition, respectively.*

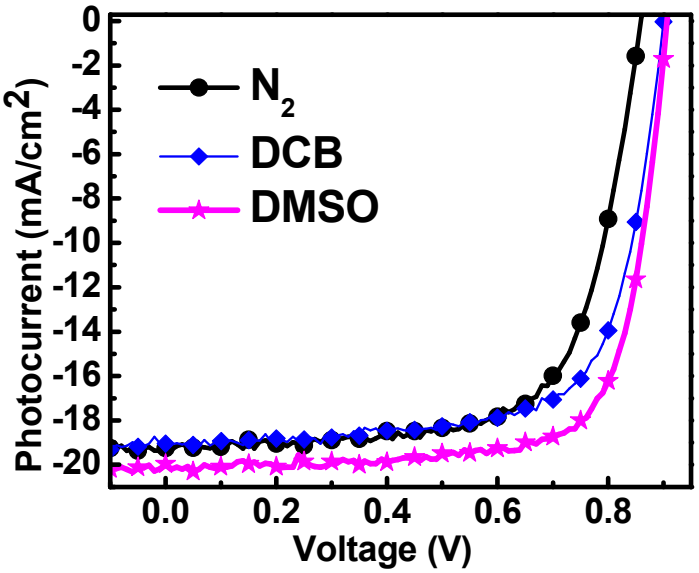

Figure 4 *Photocurrent (J) versus Voltage (V) curves for solar cells fabricated under atmosphere of N_2 and DCB, and DMSO vapors, respectively.*

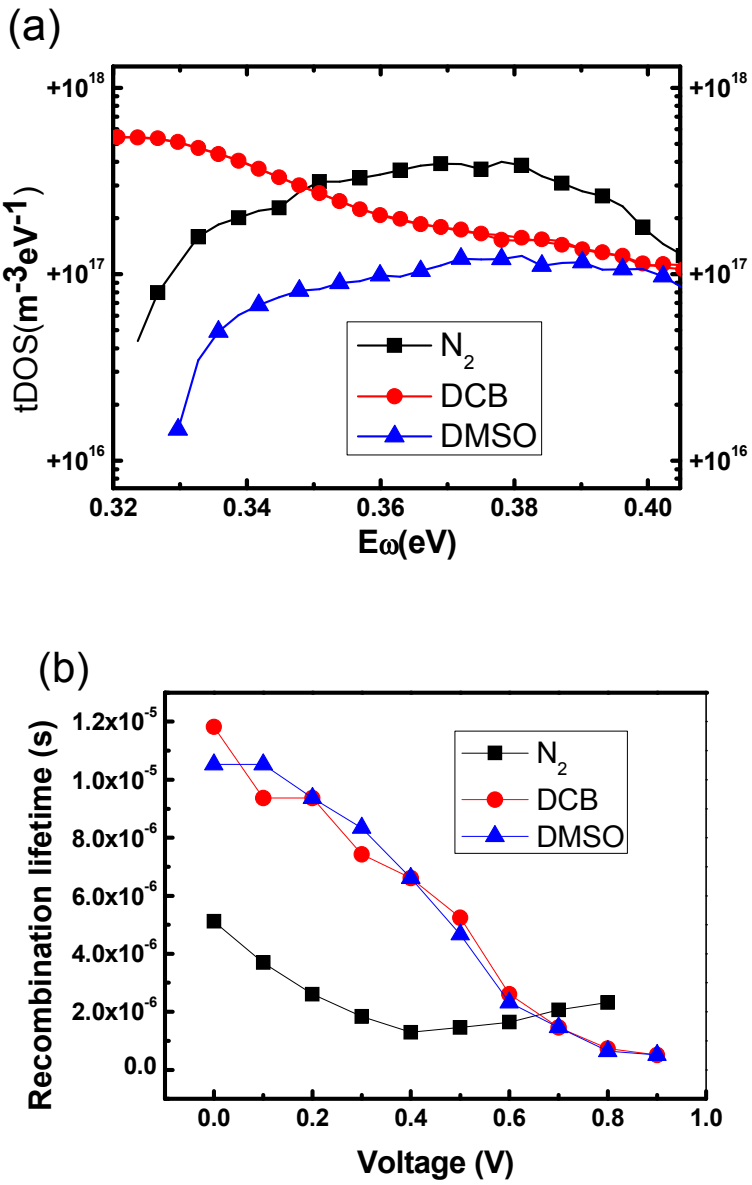

Figure 5 *(a) Trap-density of states measured from the thermal admittance spectroscopy measurement, and (b) Carrier recombination lifetime of the devices with perovskite films treated by N_2, and DCB, and DMSO vapors.*

Highlight of manuscript

Organic solvent vapor introduced during the formation of hybrid perovskite films changes the grain orientation and reduces charge recombination.